Propagation Measurements and Analysis on MF and HF Bands in Urban Areas in The Netherlands

Koos Fockens, Robert Vogt-Ardatjew, and Frank Leferink, *Fellow, IEEE*

***Abstract*—Using a new propagation measurement set-up, which produces a high number of data, enabling a proper statistical analysis, and resulting in very concise results, propagation measurements were performed and analyzed at 16 residential locations in The Netherlands in the frequency range from 1.8 to 28 MHz. In the whole frequency range the propagation loss appears to be higher than might be expected according the International Telecommunication Union ground-wave propagation model. Also typical characteristics of that model are not present, but instead the propagation shows a constant roll-off in dBs per decade, with a slope increasing with frequency. A regression curve could be established, and constants filled in. This statistical information may be used for building an accumulation model to lay a causality between source powers, source densities, and local man-made noise levels.**

***Index Terms*—Accumulation of man-made radio noise (MMN), electromagnetic compatibility (EMC), propagation.**

I. Introduction

In a study on the accumulation of man-made radio noise (MMN) by large numbers of noise sources, the propagation of the EM waves from individual noise sources to a point of aggregation is very relevant. MMN in the frequency range of 0.47 to 50 MHz was investigated earlier [1]. A further statistical study of the measurement results revealed that there is a strong correlation between the measured noise floor and the density of habitation [2]. These results raise the question of how does the radio noise propagate in these populated areas, and what is the propagation loss with distance. In the earlier mentioned frequency range, the wavelength vary from 6 to 600 m. As the field strength (FS) measurements were done at an antenna height of 2 m, and the sources are located in homes mostly at the first, second or third floor, or in more dense areas in higher apartment buildings, these heights are also relatively low.

Manuscript received August 24, 2021; revised November 8, 2021; accepted December 12, 2021. Date of publication February 1, 2022; date of current version June 13, 2022. *(Corresponding author: Koos Fockens.)*

Koos Fockens is with the University of Twente, 7522NB Enschede, The Netherlands, and also with the EMC/EMF Committee of the Dutch Radio Amateur Society, 6801BD Arnhem, The Netherlands (e-mail: t.fockens@utwente.nl).

Robert Vogt-Ardatjew is with the University of Twente, 7522NB Enschede, The Netherlands (e-mail: r.a.vogtardatjew@utwente.nl).

Frank Leferink is with Thales Netherlands, 7554RR Hengelo, The Netherlands, and also with the University of Twente, 7522NB Enschede, The Netherlands (e-mail: leferink@ieee.org).

Color versions of one or more figures in this article are available at https://doi.org/10.1109/TEMC.2021.3137237.

Digital Object Identifier 10.1109/TEMC.2021.3137237

So, a very reasonable presumption is that the propagation may be described by the theory of the ground-wave (GW) propagation.

For a good understanding of this theory we will look into a part of the history. After Marconi had proven the ability of long range radio communication by his transatlantic experiments in 1901 the need for a theoretical explanation was first fulfilled by Zenneck [3] and Sommerfeld [4]. Zenneck introduced a surface wave as a solution for the Maxwell equations. Sommerfeld analyzed the case of a vertical Hertzian dipole over a lossy ground, and came also to the surface wave as described by Zenneck, hereafter called "zenneck surface wave" (ZSW). The main property of this ZSW is that the energy is trapped on the surface, and that the roll-off with distance is 10 dB/decade, instead of 20 dB/decade for a wave in free space. Starting in 1936 Norton showed in [5]–[7] that the ZSW could only exist under extreme conditions, and that Sommerfeld had made a mistake in his theory by a faulty interpretation of the square root of a complex variable, this resulting in the so-called "sign controversy." A complete overview of this history can be found in [8] and [9].

Norton defined in [10] the GW as "A Radio Wave that is propagated through space and is, ordinarily, affected by the presence of the ground," with excluding any other reflections than against ground, as for example the ionosphere. In his solution the FS at a distance from a transmitting antenna, a vertical dipole or a magnetic loop with the winding in a vertical plane, is given by an equation in [10], showing a sum of three terms. The three terms are corresponding respectively to the direct wave, the ground reflected wave, and the surface wave, generally called the "Norton Surface Wave," NSW. In the derivation by Norton the NSW is mathematically the result of the subtraction of the optically reflected wave from the total of wave energy that is interacting with the ground. When the transmitting and the receiving antenna are close to the ground with respect to the wavelength the direct and the reflected wave will cancel, so the NSW is left. It is important to realize that the NSW is not trapped on the surface, in contrast to the ZSW, and that the roll-off with distance is minimal 20 dB/decade of distance. The values of the attenuation can be looked up on graphics in [11], a description is given in [12], and may be calculated by means of [13].

In this article, propagation in urban areas, all three wave paths in the GW theory are involved. The distance varies from 50 to 1000 m. In the measurements the transmitter antenna is at a level of 3 m and the receiving antenna at 2 m. That means that generally the direct and reflected wave are cancelling each other, but that especially for the short distances and for the upper part

of the frequency range, the direct and reflected wave may play a role, next to the NSW. For all three paths the buildings may damp, reflect, or scatter all three waves. Especially tall vertical constructions as street lamps, towers, etc., may cause scattering, which, depending on conductivity and the ratio between height and wavelength, may cause forward, back, and random scattering. Buried conductors in the earth, like all kinds of cables and metal pipes, may enhance the ground conductivity, so decrease the attenuation of the surface wave. This is especially the case at the lower frequencies with the greater skin depth. Also overhead cables may cause a considerable increase of propagation, but the mechanism is very different from propagation by cables in the ground. We must remark here that overhead cabling is not used in The Netherlands, so does not play a role in our measurements.

In the last decades propagation studies, theoretically and empirical [14], [15], are mostly concentrated on very high frequency (VHF) and ultra high frequency (UHF) frequencies, especially in urban areas. In this frequency range the wavelength is small to very small with relation to the dimensions of the objects in that environment. For the median frequency (MF) and high frequency (HF) range the wavelengths are larger or equal to these dimensions. This also means that in the VHF/UHF range the wave interaction with the ground is less relevant and that free space, reflected, and scattered paths dominates. As a consequence these studies are not relevant in our case.

There is a very limited number of studies about propagation in urban areas on frequencies below 30 MHz, and they are in essence limited to Medium Wave broadcasting signals. In [16], an extensive measurement campaign and theory building has been performed about the propagation from a local MW transmitter site North of London, through the city centre to the South of London, with a total range of 60 km. Three frequencies were involved, and interesting phenomena were recorded and theoretically explained. Herein the built-up environment with its buildings was modeled as a "bed of nails" like structure. However, in our study the relevant frequency range is higher, and the distance much shorter. In [17], FS measurements were performed on the propagation of a local MW transmitter in São Paulo, Brazil. One of the results that were reported is: "the prediction model of Rec. ITU-R P.368-9 overestimates the measured field during daytime." Consequently the GW propagation losses were higher than expected. In [18], propagation measurements on HF frequencies were reported in open desert areas, as well as in urban environments. The conclusion in this article were that the losses in open areas matched the expectation within a few dB, but in urban areas a diversity of propagation losses was found when measured the GW propagation path, and varied all over the city. A need was concluded to develop a prediction model for urban environments. Lichun [19] reports a new MF and HF GW propagation model for urban areas. It includes a fundamental addition to the Norton model by building-complex parameters and height-gain factors. The model applies for areas with high and tall buildings in particular. Only validating measurements at the medium wave frequencies were reported.

We conclude that the existing models for propagation below 30 MHz handle urban areas as a local disruption in a wider area, mainly for the purpose of coverage studies of broadcasting transmitters. For our application, being short range intra-urban propagation of man-made noise in the MF and HF range, there is no sufficient scientific information available about measurement data, nor theoretical models, useful for a statistical modeling of accumulation of spatial spread noise sources, so leading to a conclusion that a measurement campaign was necessarily.

TABLE I
OVERVIEW OF MEASUREMENT LOCATIONS

Location			Number of homes in radii of the annuluses [meter]							Environment	
No.	Call sign	City	0-50 [m]	50-100	100-200	200-300	300-400	400-500	Total	Type	Group
1	PA0RLM	Driebergen	6	2	48	108	258	249	671	Rural	I
2	PA3AWN	De Heurne	3	10	11	35	26	23	108	Res. 1	
3	PA0RYL	Huis ter Heide	5	15	98	147	54	49	368	Res. 1	
4	PA0JMG	Drachten	7	7	66	110	107	130	427	Res. 1	
5	PA0WTA	Apeldoorn	6	14	62	225	261	225	793	Res. 1	
6	PA0HTT	Ommen	12	54	153	176	144	112	651	Res. 2	II
7	PC7M	Goor	23	43	158	133	158	193	708	Res. 2	
8	PA0VBR	Nijmegen	27	71	160	184	338	379	1159	Res. 2	
9	PC0WP	Hengelo(Ov)	11	39	108	358	313	423	1252	Res. 2	
10	PA1AT	Assen	24	63	152	382	406	308	1335	Res. 2	
11	PB0AIR	Hengelo(Ov)	31	64	366	363	447	626	1897	Res. 2	
12	PA0WJG	Nieuwegein	22	55	348	540	446	518	1929	Res. 2	
13	PA0RSM	Amersfoort	30	86	210	407	323	452	1508	Res. 3	III
14	PA3BME	Driebergen	21	94	274	446	407	441	1683	Res. 3	
15	PA3GXD	Meppel	52	106	369	511	533	575	2146	City	
16	PH1E	Eindhoven	34	57	274	448	656	715	2184	City	

The rest of this article is organized as follows. In Section II we describe the measurement methods, in Section III the data processing and some theoretical aspects. Section IV describes the statistical analysis and the results thereof. Finally, Section V concludes this article. In Appendix 1, we describe validation measurements, and in Appendix 2 we calculate the FS above perfect electrical conducting (PEC) ground. At the end Appendix 3 derives the equations to make FS measurement corrections in the near field.

II. DESCRIPTION OF THE MEASUREMENTS

The goal of the measurement campaign is to gather statistical data about transmission loss as a function of distance, frequency, and of density of habitation. Thereto we need measurements on several locations in diverse environments. From the list of measurement locations, earlier used in [1], we selected a number of 16, and enumerates them in Table I.

They all belong to contributing radio amateurs, the locations are coded in the table and further on in accordance with their radio call signs. Also the city is given and numbers of homes around that locations. The type of environment is given as defined in [1], and listed as follows.

1) Quiet Rural *Area*: No residences, no infra structures within 1.5 km radius.
2) Rural *Area*: up to 10 residences within a radius of 100 m, but at a distance of at least 100 m outside built-up area.
3) Residential *Area*-1: 11–50 residences within 100 m.
4) Residential *Area*-2: 5–100 residences within 100 m.
5) Residential *Area*-3: $>$100 residences within 100 m.
6) City *Area*: large apartment buildings, commercial and city centers:
   a) residences directly surrounded by shops and other city center activity; or
   b) the number of residences within a radius of 100 m is larger than 150; or

c) the number of residences within a radius of 500 m is larger than 2000.

The location groups, as given in Table I, are based on the types residential 1–3, but supplemented with one rural (location no. 1, which literally fulfills the definition of type rural, but is enclosed in urban area), and for group 3 the residential type 3 is supplemented with two location from the city type. The decisions here and the cut-offs are based on a study of the topographic maps of the locations, resulting in heuristic decisions. The measurement locations are in The Netherlands, and so have some restrictions. First, the areas are all flat, and secondly, the focus is primary on the civil HF listeners/users, they mostly live in residential areas. Metropole-like city centers with large numbers of high-rise buildings are not included.

The principle of the measurements is based on placing a low power beacon transmitter at a fixed location and drive with a mobile FS measurement system in a fixed traject from that location away up to a distance of about 1 km and back via a different path, depending on the local topography, and selectively measuring the FS generated by that beacon transmitter. This drive is repeated for all test frequencies over the same trajectory: 1.85 (160 m wavelength); 3.57 (80 m); 7.07 (40 m); 14.07 (20 m); 21.07 (15 m); and 28.07 MHz (10 m). During the drive repeatedly measurement samples are taken at random varying distances 8–16 m between themselves, resulting in a high number of samples.

The special designed beacon transmitter consists of a 19 inch cabinet, a 4 m high rod antenna, and two metal plates forming a counterpoise grounding, see Fig. 1. Next to the transmitter, a commercial Elad FDM-DUO SDR transceiver, the cabinet contains an antenna matching circuit and a Morse code ID generator, which modulates the transmitter carrier in Frequency Shift Keying with a shift of 100 Hz. That is well within the bandwidth of the measurement receiver, so that the measurement is not disturbed by the ID transmission. The transceiver output power is set at 1 W. The RF carrier is measured at the measurement receiver. In principle this includes noise within the receiver bandwidth, but during the measurements the level of the beacon signal is that strong that external and internal noise does not contribute to the measurement result significantly.

For calibration the FS has been measured at a distance of 25 m on a flat and undisturbed piece of grass land by using a calibrated magnetic antenna, the Rohde and Schwarz Z2 loop antenna. For the near field (lower frequencies) corrections were made according correction factors, derived in Appendix 3. Also for ground losses (upper frequencies, very small) compensations, calculated with GRWAVE [13], has been calculated and applied. From these measurements the actual effective isotropic radiated power (EIRP) has been calculated for each test frequency. The EIRP values are to be used as calibration numbers in the post-processing of the FS measurements.

The mobile FS measurement system was build in a passenger car. On the roof an active E-field antenna system is mounted, see Fig. 2. The antenna groundplane as shown is well grounded on the roof and the bodywork of the car by a low impedance capacitive coupling through two self-adhesive copper strips on the roof, behind the luggage carrier strips. The capacitance per strip is 10 nF. Fig. 4 shows the principle diagram of the measurement system, and Fig. 3 the equipment inside the car.

Fig. 1. View of the beacon transmitter.

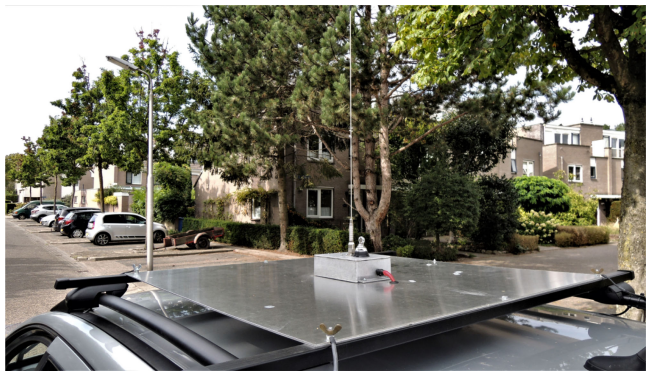

Fig. 2. Measurement antenna system.

The calibration of the mobile FS measurement system has been carried out for the system as a whole, including the car. The reference antenna method has been used, using the same Rohde and Schwarz EZ2 loop antenna as a reference as also used for calibration the transmitter. A beacon transmitter at a distance of 40 m produced a vertical polarized test signal.

Fig. 3. Measurement equipment.

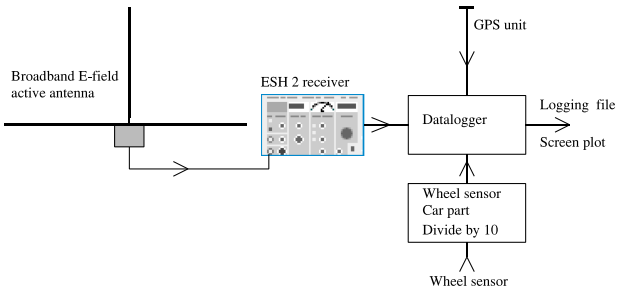

Fig. 4. Set-up of the mobile FS measurement system.

The reference antenna was positioned at the same height as the E-field antenna on the car. For the frequencies, where the E- and H-field diverge because of the effect of the near field, a compensation has been made, see Appendix 3. Also the directivity of the mobile set-up has been measured at 5 directions from 0° (front) to 180° (back of the car). For all test frequencies a small difference in antenna factor was observed, maximal sensitivity for a signal arriving at the front of the car, and a minimum in the sensitivity for signals arriving from the back side of the car. The amplitude of this directional variation is lowest at 1.8 MHz: 0.3 dB, and highest at 25 MHz: 1.3 dB. For each test frequency a cosine function approximation has been derived. An algorithm has been developed to estimate the direction of arrival of the beacon signal during the measurement drives from the GPS data, using the stored location of the beacon, so to compensate for directional variations in the antenna-factor in real time.

For validating the measurement system and method measurement drives has been performed in flat and open areas as described in Appendix 1. Concerning seasonal effects on the propagation loss, monthly measurements were carried out throughout a full year, from September 2019 to November 2020, on a fixed traject, partly in populated area, and partly over open land. A clear relation with seasonal variation in soil humidity was found, but the maximal deviation from the median on the loss measurement, as caused by a total of 10% to 90% spread, was very limited, and varied from 1 (1.8 MHz) up to 3 dB (28 MHz). As a result no corrections were applied in our urban measurements.

III. Data Processing

A. Decimation of Samples and the Statistical Approach Thereof

For the purpose of the accumulation study an estimator is required in this experiment that is representing the propagation loss. We take here the expected value from the probability distribution function (pdf) of the propagation loss, thus the mean value μ in the pdf.

But actually, samples of FS levels are measured and normalized for an EIRP of 1 W. These FS levels are used as an intermediate result, they can be used to compare with the FS levels that are resulting from calculations according the ITU GW propagation model.

In the postprocessing the measurement samples are grouped into bins, representing ranges of distances. The samples, inputted in those bins, can be measured on a single location, on a group of locations, or on all locations. They may be combined during the postprocessing in those bins. In this way a kind of parallel processing is achieved from: first the individual locations, second the three groups of locations with comparable density of habitation; and third from all measurement locations totalized together.

From each bin an average value Av and a median value Me from N samples can be calculated. Generally, Av appear to equal μ nearly in the measurement results. For higher numbers of $N\,\mathrm{Av}$ and Me approach the pdf mean, and so the mean value μ. In this case we use the linear values of the FS e for the statistical calculation, and the results are converted back in logarithmic values E [dBμV/m]. The statistical processing is complicated by the fact that we need to convert FS values into a linear quantity, μV/m, on which we can apply the statistics. Further arithmetics and presentations are usually done in logarithmic quantities, e.g., in dBμV/m (FS) or dB (propagation loss). For the average and median values this is not a problem as they can be converted from linear quantities into dBs and vice versa unambiguously. But, deviations translate from linear into logarithmic values for a negative and for a positive deviation differently. This makes it necessarily to define and describe the complete processing procedure.

Each bin delivers an average value e_{Av}, $E_{\mathrm{Av}} = \log e_{\mathrm{Av}}$ and an estimated standard error e_{SE}. The error will be split up in the logarithmic quantities $E_{\mathrm{SE}+}$ and $E_{\mathrm{SE}-}$

$$E_{\mathrm{SE}+} = 20 * \log\left(\frac{e_{\mathrm{Av}} + e_{\mathrm{SE}}}{e_{\mathrm{Av}}}\right) \tag{1}$$

$$E_{\mathrm{SE}-} = 20 * \log\left(\frac{e_{\mathrm{Av}} - e_{\mathrm{SE}}}{e_{\mathrm{Av}}}\right). \tag{2}$$

Herein is $E_{\mathrm{SE}+} \geq 0$, $E_{\mathrm{SE}-} \leq 0$, and because of the asymmetry in the ratios $|E_{\mathrm{SE}-}| \geq E_{\mathrm{SE}+}$. The median FS value E_{Me} has to be normalized for an effective radiated power from the

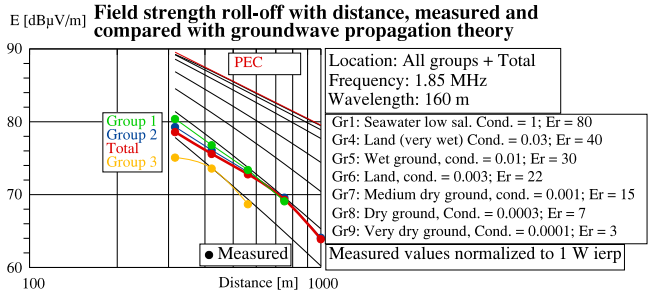

Fig. 5. Normalized measured FS levels compared with calculated values according existing models, 1.85 MHz. Notice: the curve Gr1 for seawater is fully covered by the PEC curve, and so invisible.

beacon transmitter of 1W

$$E_{N,\mathrm{Me}} = E_{\mathrm{Me}} - P_{\mathrm{tx}}\,[\mathrm{dB}W] \tag{3}$$

where P_{tx} is the EIRP as measured by the calibration of the beacon transmitter. To calculate the propagation loss L the FS median is subtracted from the FS that would be measured when the ground is PEC

$$L_{\mathrm{Me}} = E_{\mathrm{PEC}} - E_{N,\mathrm{Me}}[\mathrm{dB}] \tag{4}$$

$$l_{\mathrm{Me}} = 10^{(L_{\mathrm{Me}}/20)}. \tag{5}$$

Because of the sign in (4) the standard errors in L will be reversed

$$L_{\mathrm{SE}+} = E_{\mathrm{SE}-}\,(\leq 0) \tag{6}$$

$$L_{\mathrm{SE}-} = E_{\mathrm{SE}+}\,(\geq 0)\,. \tag{7}$$

Inversely, the linear standard error in the propagation loss is

$$l_{\mathrm{SE}} = l_{\mathrm{Me}}\left(1 - 10^{(L_{\mathrm{SE}+}/20)}\right) \tag{8}$$

$$= l_{\mathrm{Me}}\left(10^{(L_{\mathrm{SE}-}/20)} - 1\right). \tag{9}$$

In this way we arrive at the same value for both polarities of l_{SE}, so one calculation suffice. In the graphics we use a dB scale, so there the both dB values $L_{\mathrm{SE}+}$ and $L_{\mathrm{SE}-}$ are used.

B. FS Measurement Results

The recorded measuring results are processed according the sub-section above, per group of locations and per frequency. First we consider the FS results, normalized to an EIRP of 1 W. In Figs. 5–8, the normalized median values of the measured FS levels are plotted for the three groups of locations and all locations totalized. Also the calculated FS values for PEC and for seven types of ground according [11] are shown. We learn from the plots that the measured FS values are nearly all below or around the calculated values for very dry ground, the least conducting type of ground in the ITU GW propagation model. Also we notice that the measured levels are lower with increasing density of habitation and decrease with frequency. Compare these figures with the results of the validation measurements, as reported in Appendix 1, Figs. 18–20. In these plots the measured FS levels are all within the range of the ITU GW model. We may

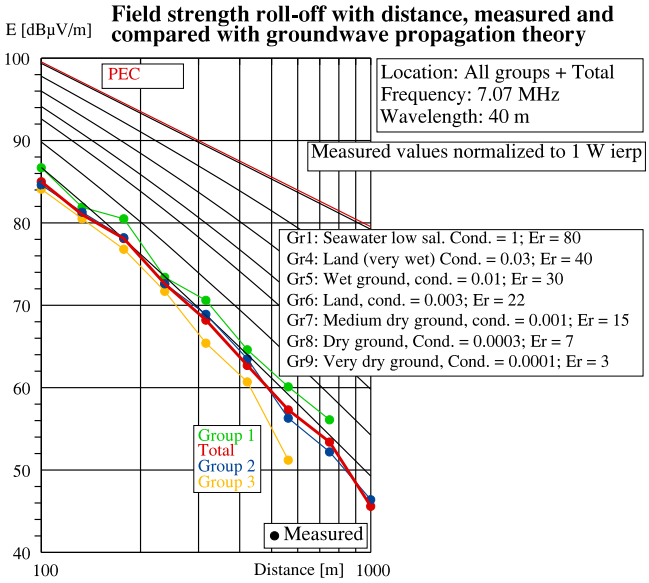

Fig. 6. Normalized measured FS levels compared with calculated values according existing models, 7.07 MHz.

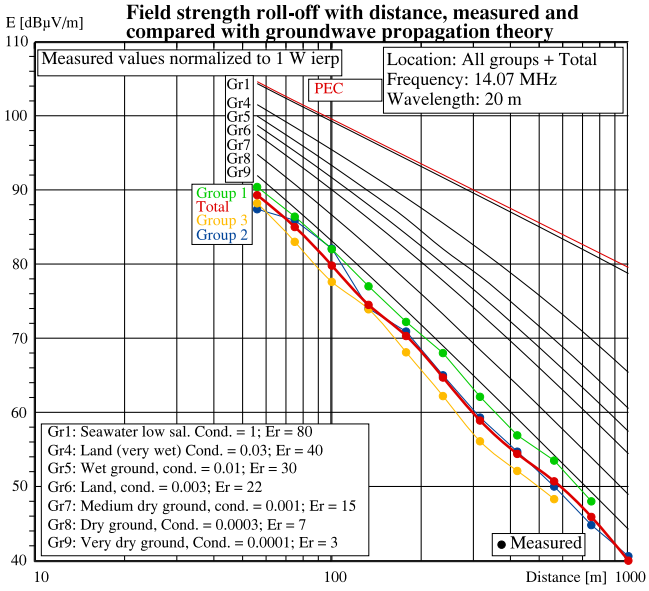

Fig. 7. Normalized measured FS levels compared with calculated values according existing models, 14.07 MHz.

conclude from our measurement results that the propagation loss in urban areas is higher than what is expected from the ITU GW model.

C. Estimation of the Propagation Pdf

Next step is to estimate the propagation pdf from the measurement samples for each bin j. We use the t-statistics for an estimation as educated in [21]. By this estimation we look for an expectation value for the mean of the population of the loss l by taking the average or median value of the samples of l:$l_{\mathrm{ME},j}$.

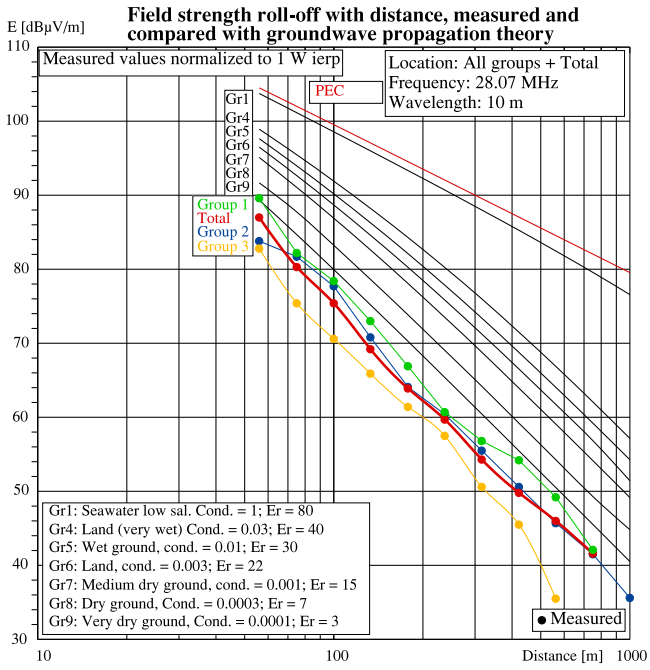

Fig. 8. Normalized measured FS levels compared with calculated values according existing models, 28.07 MHz.

For the point estimate μ we calculate

$$l_{\mu,j} = l_{\mathrm{Me},j} \pm t * l_{\mathrm{SE},j} \text{ wherein } t = 0 \tag{10}$$

$$= l_{\mathrm{Me},j} \tag{11}$$

$$L_{\mu,j} = 20 * \log l_{\mu,j}. \tag{12}$$

From the estimated standard error in the propagation loss, we want to determine the confidence interval (CI), wherein $t \in \mathrm{CI}$. Accepting the middle 90% of the distribution, 10% is left on both trails together, so $p = 0.10$. For degrees of freedom $df = n - 1$ we look up a value for t_j in the *t*-distribution table in [21]. The lower and upper end of the CI of $l_{\mu,j}$ is now given by

$$l_{\mu_{\mathrm{lower}},j} = l_{\mathrm{Me},j} - t_j * l_{\mathrm{SE},j} \tag{13}$$

$$l_{\mu_{\mathrm{upper}},j} = l_{\mathrm{Me},j} + t_j * l_{\mathrm{SE},j} \tag{14}$$

$$L_{\mu_{\mathrm{lower}},j} = 20 * \log l_{\mu_{\mathrm{lower}},j}[\mathrm{dB}] \tag{15}$$

$$L_{\mu_{\mathrm{upper}},j} = 20 * \log l_{\mu_{\mathrm{upper}},j}[\mathrm{dB}]. \tag{16}$$

These postprocessing calculations were executed in a dedicated software program, written in C. Herein are the median FS values in each bin used as a basis for the propagation loss calculations, instead of the average values.

D. Theory and the Calculations of the Propagation Loss

In Appendix 2 the FS roll-off is calculated over a PEC ground. For distances d in the far field region and larger than the height of the transmitter and receiver antenna the FS values are approached by

$$e_{\mathrm{PEC},d} = \frac{2}{d}\sqrt{(p_{\mathrm{tx}}/2) \cdot g_{\mathrm{dip}} \cdot 30} = \frac{1}{d}\sqrt{p_{\mathrm{tx}} \cdot 90} \tag{17}$$

wherein d is the distance from transmitter to measurement location, p_{tx} is the EIRP, and g_{dip} the gain of a dipole antenna. Several kinds of transmission loss are defined in [20]. However, for calculating interference risks as in relevant CISPR electromagnetic compatibility (EMC) standards often the propagation characteristics of free space is used, resulting in a 20 dB roll-off per decade of the distance. So for reference it is relevant to know the increase of transmission loss with distance for the free space condition.

Under far field condition, assuming an electrical dipole as transmitting antenna, we calculate the free space power density s_{fs} and the FS e_{fs} as

$$s_{\mathrm{fs}} = \frac{p_{\mathrm{tx}} \cdot g_{\mathrm{dip}}}{4\pi d^2} \tag{18}$$

$$e_{\mathrm{fs}} = \sqrt{s_{\mathrm{fs}} \cdot Z_0} \approx \frac{1}{d}\sqrt{p_{\mathrm{tx}} \cdot 120\pi/4\pi} \tag{19}$$

$$\approx \frac{1}{d}\sqrt{p_{\mathrm{tx}} \cdot 1.5 \cdot 30}. \tag{20}$$

The free space propagation loss[1] L_{fs} we calculate from (20)

$$L_{\mathrm{fs}} = E_{d=1} - E_d[\mathrm{dB}] \tag{21}$$

$$= 20 \cdot \log\left(\frac{\sqrt{p_{\mathrm{tx}} \cdot 1.5 \cdot 30}}{1}\right) - 20 \cdot \log\left(\frac{\sqrt{p_{\mathrm{tx}} \cdot 1.5 \cdot 30}}{d}\right) \tag{22}$$

$$= 20 * \log(d). \tag{23}$$

From our measured FS levels we want to calculate the "excess propagation loss" by comparing with the FS calculated for PEC ground and with ITU ground type "land" [11], [12] with a mediate conductivity of 3 mS/m and relative permittivity of 22. From (4)

$$L_{\mathrm{excess\_PEC}} = E_{\mathrm{PEC}} - E_{N,\mathrm{Me}}[\mathrm{dB}] \tag{24}$$

$$L_{\mathrm{excess\_Land}} = E_{\mathrm{Land}} - E_{N,\mathrm{Me}}[\mathrm{dB}] \tag{25}$$

Limited to the far field ranges, we may calculate the full propagation loss L_{full} by

$$L_{\mathrm{full}} = L_{\mathrm{excess\_PEC}} + L_{\mathrm{fs}} \tag{26}$$

$$= L_{\mathrm{excess\_PEC}} + 20 * \log(d). \tag{27}$$

IV. Statistical Result Analyses

Applying the foregoing calculations on the measurement results are resulting in the Figs. 9–11 for resp. 1.85, 7, 14 and 28 MHz. In those plots the processing results are collected for the three groups of locations with increasing density of habitation, and for all locations totalized. Notice that the excess propagation loss curves related to "land" show a transition from increasing to constant at a distance related to the wavelength. We find this transition distance back in GW FS curves in [11], where

[1]Here with "propagation loss" we only consider the effect of roll-off with distance of the field strength. Transmission loss as defined in [18] also takes into account the aperture of the receiving antenna, which is frequency dependent. It is defined as a ratio between the radiated power, ierp, and the received power from the lossless receiving antenna.

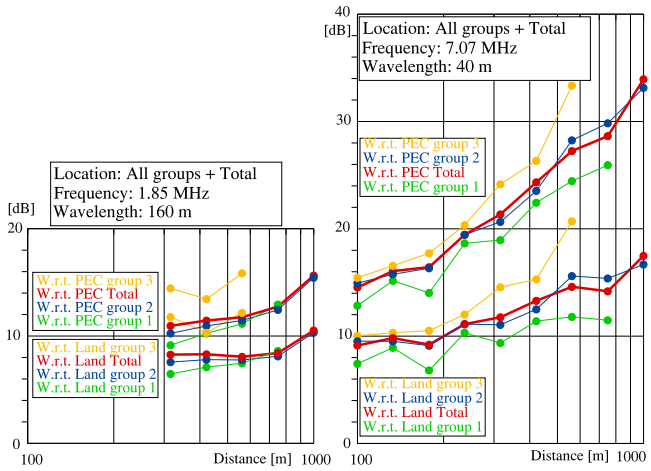

Fig. 9. Excess propagation loss curves for 1.85 and 7 MHz.

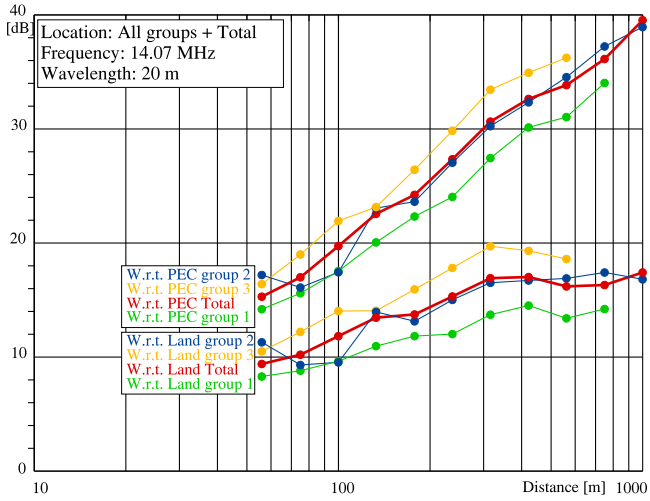

Fig. 10. Excess propagation loss curves for 14 MHz.

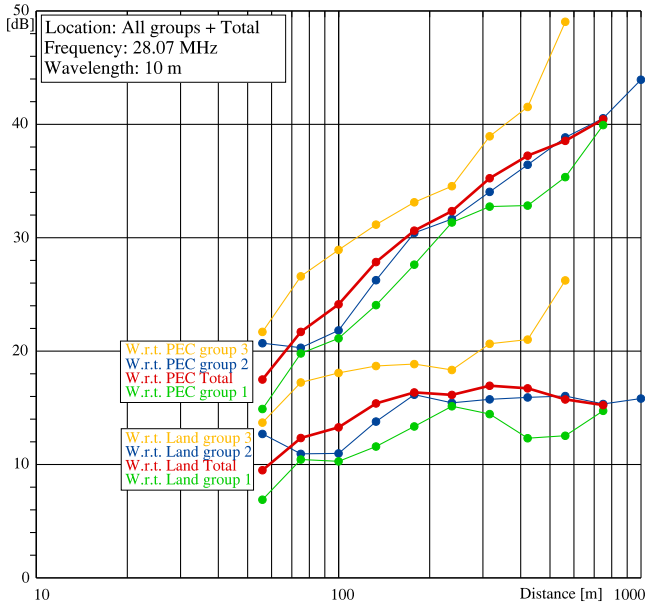

Fig. 11. Excess propagation loss curves for 28 MHz.

a transition in the roll-off from 20 to 40 dB/dec. takes place. This transition is characteristic for GW propagation model, see [5] and [11]. For example, at a wavelength of 20 m the transition is at a distance of approximately 300 meters, about 15 times the wavelength. In Fig. 10 we find this transition back in the curves which compare the measured excess propagation loss with the propagation loss according ITU GW "land" model. Here, we find the bend, while comparing with the linear PEC line we find no bend. In Fig. 9, concerning frequencies 1.85 and 7.07 MHz, wavelength resp. 160 and 40 m, these transition distances are over 1000 m, so out of range in these plots. We may conclude from the plots in Figs. 9–11 that propagation in residential areas does not follow the ITU GW propagation model, but instead follow a constant slope with a constant number of dBs per decade of distance.

A. *Regression Analysis: Correlation to a Straight Line and its Slope*

Inspecting the measurement results leads to the conclusion that the extra path loss above the loss according to GW propagation over PEC, in relation to the logarithmic value of the distance, is well approached by a straight line. For considering a correlation with a straight line we may write

$$L_{\text{full}} = \text{slope} * D + a. \tag{28}$$

Now, we arrive at a linear relation between L_{full} in dB and $D = 20 * \log(d)$. With this relation we assume a case of interval measures, implying we may apply the Pearson correlation test, using the Pearson product-moment coefficient [21]. Here, a measurement ensemble consists of the measurement results on a single frequency band on a number n of distances as samples $i = 1$ to $i = n$. In this article, n varies from 3 to 11.

As mentioned before we want to compare our measurement results with the free space roll-off with distance of 20 dB/dec., starting at the reference distance of 10 m. This means that we must force the regression line going through the point $L_{\text{full}} = 20$ dB and $D = 20 * \log(d) = 20$. So $\alpha = 0$ for slope $= 1$ (= 20 dB/dec.). We can arrange that by, instead of the average values for L_{full} and D (27), (28), substitute $av\_L_{\text{full}} = 20$ and $av_D = 20$ in the formula for the slope of the regression line (30)

$$\text{slope} = \frac{\sum_{i=1}^{n} (D_i - av\_D) * (L_{\text{full},i} - av\_L_{\text{full}})}{\sum_{i=1}^{n} (D_i - av\_D)^2} \tag{29}$$

$$= \frac{\sum_{i=1}^{n} (D_i - 20) * (L_{\text{full},i} - 20)}{\sum_{i=1}^{n} (D_i - 20)^2}. \tag{30}$$

The degrees of freedom is now given by $df = n - 1$, one higher than in the standard Pearson correlation test, as one fixed sample point has been added. n is the number of bins involved.

The calculations has been performed for all three groups of locations and for all locations totalized. We show here the results for all locations totalized only and for four frequencies. Figs. 12–16 are resulting. We find a high correlation coefficients r and roll-off slope of 26.6 to 43.1 dB/dec. of the distance.

All resulting values for the Roll-Off slope are shown in Fig. 16 as a function of the frequency. Also a regression line can be

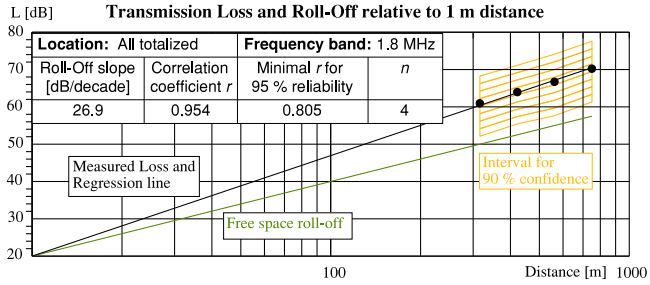

Fig. 12. Transmission loss and roll-off relative to 1 m distance at 1.8 MHz.

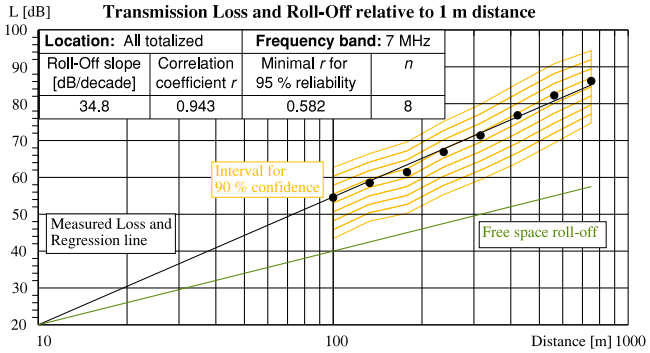

Fig. 13. Transmission loss and roll-off relative to 1 m distance at 7 MHz.

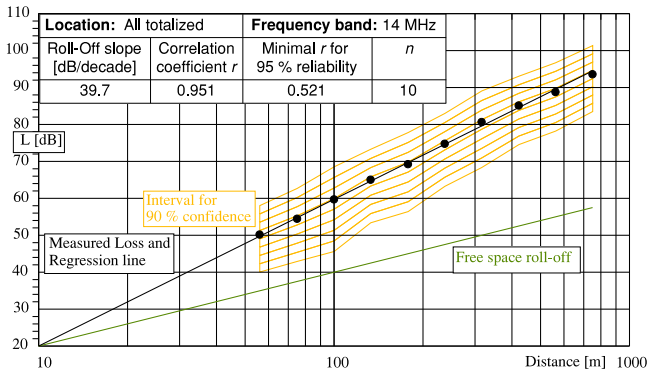

Fig. 14. Transmission loss and roll-off relative to 1 m distance at 14 MHz.

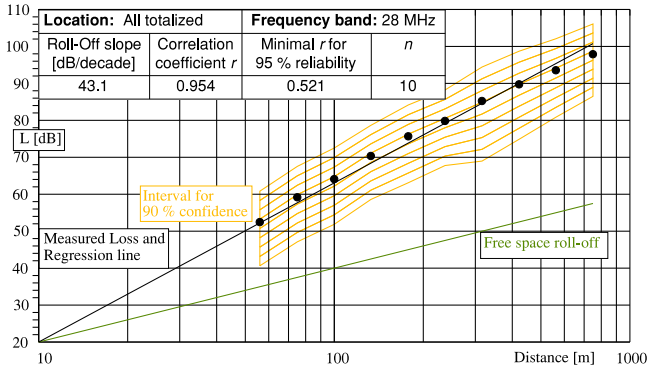

Fig. 15. Transmission loss and roll-off relative to 1 m distance at 28 MHz.

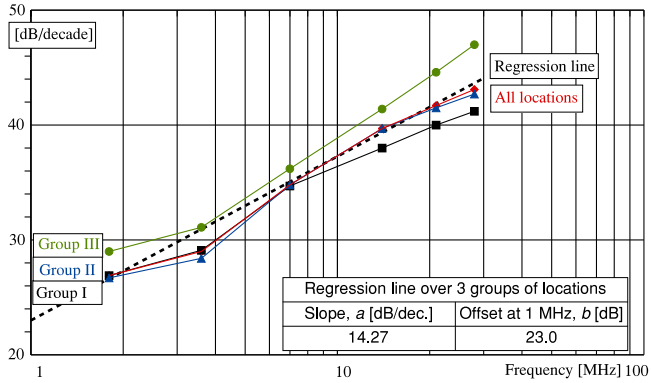

Fig. 16. Roll-off slope as a function of frequency. Results from the three groups and all locations together.

TABLE II
ROLL-OFF SLOPE AS FOUND BY MEASUREMENT IN THE NETHERLANDS

Frequency range 1 - 30 MHz	*Roll-Off slope* = *a**log(*f* [MHz]) + *b* [dB/decade]				
Correlation over:	*n*	*r*	r_{min}	*a*	*b*
Group I + II + III	**18**	**0.963**	**0.378**	**14.3**	**23.0**
Low density area, group I	6	0.994	0.622	12.6	23.3
Median density area, group II	6	0.989	0.622	14.6	22.1
High density area, group III	6	0.992	0.622	15.6	23.7
All locations	6	0.993	0.622	14.5	22.4

drawn here, which leads to a general approximation of the FS roll-off with distance for frequencies between 1 and 30 MHz.

The result is summarized in Table II. We consider the numbers for Group I+II+III in Table II as the main outcome. It is composed of the results from the correlation of propagation loss with distance for six frequencies from all location groups, so giving eighteen samples for the correlation with frequency. See the schematic in Fig. 17, wherein an overview of the processing of the measurement data and the statistical analysis is shown. For low and high density areas additional values for a and b are given. Also is, by way of checking, all samples from all locations put together and processed, resulting in the values at the last row of Table II. These results were comparable with the values for Group I+II+III and for median density area.

V. CONCLUSION

In the study of accumulation of man-made noise on MF and HF frequencies in urban areas the propagation within these areas may play a significant role. Information from foregoing propagation studies appear to be unsatisfying, so a new experiment had to be set-up wherein a mobile FS measurement system, in combination with a stationary beacon transmitter, performed propagation measurements at a small scale with hundreds of measurement points at propagation distances up to 1000 m. This method produces a high number of data and allows to run a proper statistical analysis, giving very concise results.

From these measurements at sixteen locations in The Netherlands at six frequencies from 1.8 to 28 MHz the conclusion can be drawn that propagation in urban areas do not follow the ITU GW propagation model, but show higher propagation losses, increasing with frequency, and show a constant roll-off with

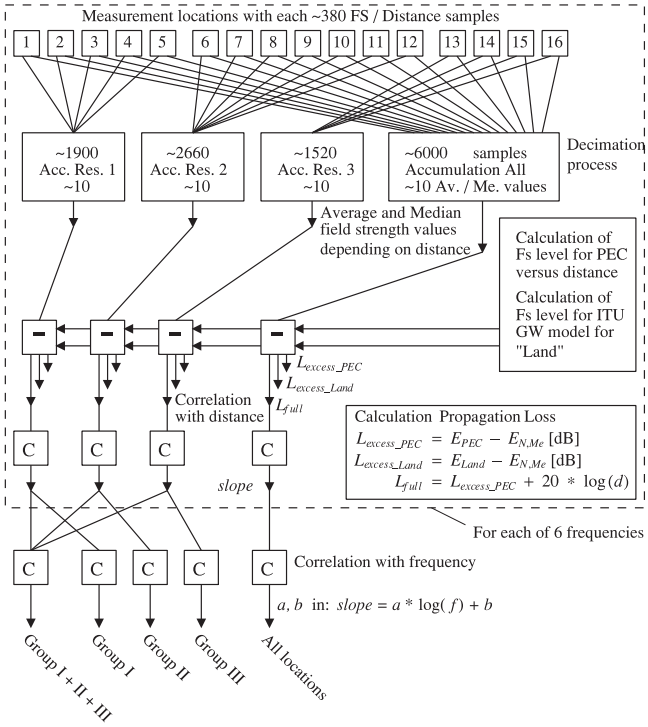

Fig. 17. Schematic overview of the data processing and analysis.

distance. The slope of this roll-off is frequency dependant according a linear regression as depicted in Fig. 16 and numerically given in Table II. Stochastically there is a small dependency on the density of habitation, as shown in the table and visible in Fig. 16, but at individual locations the local topography is strongly relevant.

The so found statistical information about propagation loss in residential areas may be used for building an accumulation model to lay a causality between source powers, source densities, and local MMN levels. We would recommend others to do propagation experiments in other urban places, using equivalent methods, to verify and broaden our results.

Appendix 1
Validation Measurements

To validate this method of measurement of the propagation loss a number of validation measurement has been carried out. By definition these measurements should be done outside residential areas in open fields where the ITU GW propagation model according [11]–[13] should apply. As the ground in residential areas has been paved for a large part, also for the reference measurements two traject with a concrete surface were sought. The three trajects, all in The Netherlands, were as follows.

1) A 3 km long, nearly straight, farmer's road near Kloosterhaar, brick road, vast open area, grown crops, only two trees halfway the road. Groundwater level: −1.2 m.
2) A 1000 m long, 25 m wide, runway of the general aviation airstrip near Drachten, asphalt concrete. Small airport building 150 m from the beacon location, business area at 150 m distance next to the runway at the far end.
3) A 2 km long, 50 m wide, decommissioned part of the 3 km runway of the military airbase Deelen, asphalt concrete, forest at 400 m distance at one side next to the runway. Dry sandy soil.

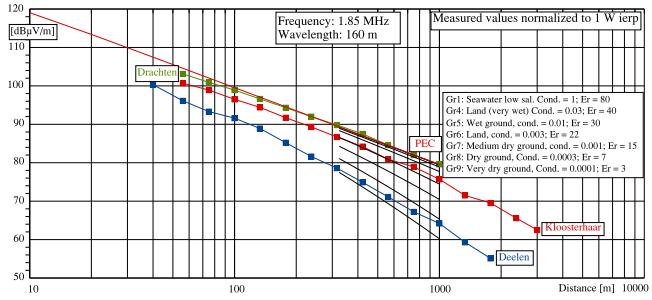

Fig. 18. FS roll-off with distance, measured and compared with ITU GW propagation model at 1.85 MHz. Notice: the curve Gr1 for seawater is fully covered by the PEC curve, and so invisible.

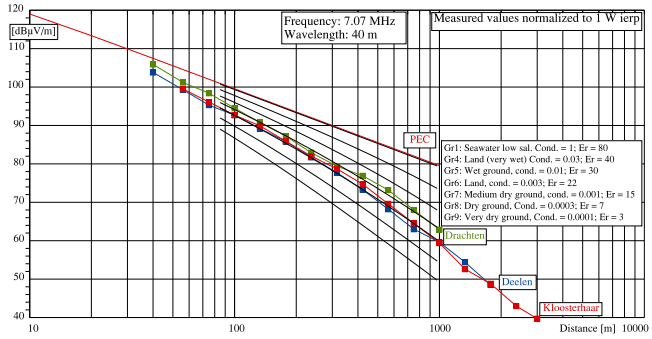

Fig. 19. FS roll-off with distance, measured and compared with ITU GW propagation model at 7.07 MHz.

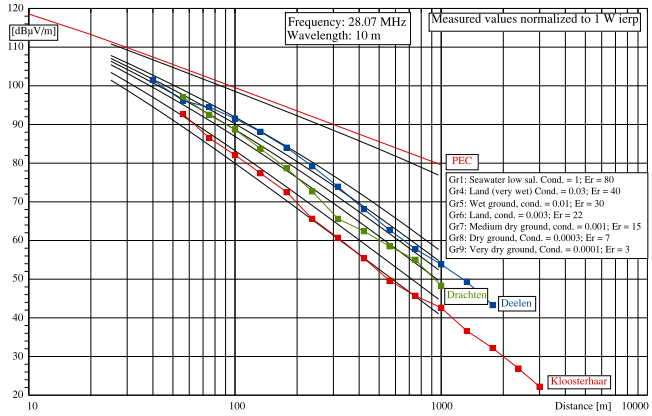

Fig. 20. FS roll-off with distance, measured and compared with ITU GW propagation model at 28.07 MHz.

The measurement results are shown as normalized FS levels next to calculated FS levels according the ITU GW propagation model for a series of standardized types of ground, and for perfect electrical conducting ground (PEC), all for an isotropic effective radiated power of 1 W. The measurements are performed at ten frequencies in the range from 1.8 to 28 MHz. Because of limited space we will show the plots of three frequencies here, showing the three locations together.

A few observations we will mention here. In the measurements at Kloosterhaar we see a good propagation for lower

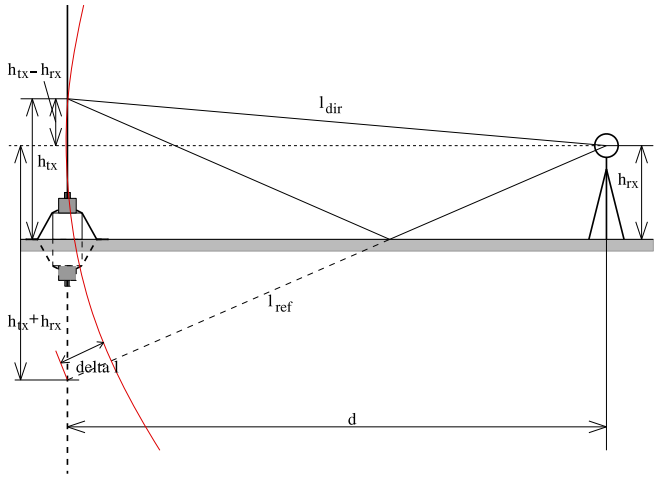

Fig. 21. Model of radiation from an asymetric dipole.

frequencies and bad propagation for the higher frequencies. We explain that by the influence of the groundwater causing an enhanced conductivity deeper in the ground, having influence at the longer wavelength. At the higher frequencies the extra losses caused by vegetation is having an effect, especially the effect of the 2 m high crops in the distance range of 200 to 700 m is visible. At Deelen the underground is sandy and dry, so bad propagation for low frequencies, but for the high frequencies the effect of the runway pavement appear to be relevant. In the measurement on the runway of Drachten the conducting effect of buried cables from decommissioned runway lighting is showing up on the lower frequencies. We conclude that these measurements show results being well inside the range we might expect, and so validate the measurement system and method.

Appendix 2
Calculation of FS Above Perfect Electrical Conducting Ground

When the antenna is elevated, for example as an asymmetric dipole (see Fig. 21), we must take into account the direct ray from transmitting antenna to the measurement antenna, and the reflected ray against ground. The reflected wave is thought to be radiated by a mirrored antenna under the ground. A simplified way, using PEC, is as follows.

When we calculate the FS using the mirror transmit antenna method, we must divide the radiated power over the two antenna parts. Further, we must apply the gain of a small electrical dipole, $g_{\mathrm{dip}} = 1.5$, for each antenna part, [22].

Direct wave

$$s_{\mathrm{dir}} = \frac{p_{\mathrm{tx}}}{2} * \frac{g_{\mathrm{dip}}}{4\pi l_{\mathrm{dir}}^2} \tag{A2.1}$$

$$e_{\mathrm{dir}} = \sqrt{s_{\mathrm{dir}} \cdot Z_0} \approx \frac{1}{l_{\mathrm{dir}}} \sqrt{p_{\mathrm{tx}} \cdot g_{\mathrm{dip}} \cdot 15} \tag{A2.2}$$

$$l_{\mathrm{dir}} = \sqrt{d^2 + (h_{\mathrm{tx}} - h_{\mathrm{rx}})^2}. \tag{A2.3}$$

Ground reflected wave

$$s_{\mathrm{ref}} = \frac{p_{\mathrm{tx}}}{2} * \frac{g_{\mathrm{dip}}}{4\pi l_{\mathrm{ref}}^2} \tag{A2.4}$$

$$e_{\mathrm{ref}} = \sqrt{s_{\mathrm{ref}} \cdot Z_0} \approx \frac{1}{l_{\mathrm{ref}}} \sqrt{p_{\mathrm{tx}} \cdot g_{\mathrm{dip}} \cdot 15} \tag{A2.5}$$

$$l_{\mathrm{ref}} = \sqrt{d^2 + (h_{\mathrm{tx}} + h_{\mathrm{rx}})^2}. \tag{A2.6}$$

The total wave is the vectorial sum of both path. Let

$$\mathrm{Re}\,(e_{\mathrm{dir}}) = |e_{\mathrm{dir}}| \tag{A2.7}$$

$$\mathrm{Im}\,(e_{\mathrm{dir}}) = 0 \tag{A2.8}$$

$$\mathrm{Re}\,(e_{\mathrm{ref}}) = |e_{\mathrm{ref}}| \cdot \cos \emptyset \tag{A2.9}$$

$$\mathrm{Im}\ (e_{\mathrm{ref}}) = |e_{\mathrm{ref}}| \cdot \sin \emptyset. \tag{A2.10}$$

Angle $\emptyset$ is caused by the delay by the extra path length $\Delta l = l_{\mathrm{ref}} - l_{\mathrm{dir}}$, vertical polarization is assumed

$$\emptyset = \frac{\Delta l}{\lambda} 2\pi \ (\Delta l \leq \lambda) \tag{A2.11}$$

$$\mathrm{Re}\ (e_{\mathrm{tot}}) = \mathrm{Re}\,(e_{\mathrm{dir}}) + \mathrm{Re}\,(e_{\mathrm{ref}}) \tag{A2.12}$$

$$= |e_{\mathrm{dir}}| + |e_{\mathrm{ref}}| \cdot \cos \emptyset \tag{A2.13}$$

$$\mathrm{Im}\,(e_{\mathrm{tot}}) = \mathrm{Im}\,(e_{\mathrm{dir}}) + \mathrm{Im}\,(e_{\mathrm{ref}}) \tag{A2.14}$$

$$= |e_{\mathrm{ref}}| \cdot \sin \emptyset \tag{A2.15}$$

$$|e_{\mathrm{tot}}| = \sqrt{(\mathrm{Re}\,(e_{\mathrm{tot}}))^2 + (\mathrm{Im}\,(e_{\mathrm{tot}}))^2} \tag{A2.16}$$

$$= \sqrt{(|e_{\mathrm{dir}}| + |e_{\mathrm{ref}}| \cdot \cos \emptyset)^2 + (|e_{\mathrm{ref}}| \cdot \sin \emptyset)^2} \tag{A2.17}$$

$$= \sqrt{e_{\mathrm{dir}}^2 + e_{\mathrm{ref}}^2 + 2 \cdot |e_{\mathrm{dir}}| \cdot |e_{\mathrm{ref}}| \cdot \cos \emptyset}. \tag{A2.18}$$

At distances larger than the transmitter and receiver antenna heights, so for $l_{\mathrm{dir}} = l_{\mathrm{ref}} = d$ and $\emptyset = 0$

$$e_{\mathrm{dir}} = e_{\mathrm{ref}} = e = \frac{1}{d} \sqrt{p_{\mathrm{tx}} \cdot g_{\mathrm{dip}} \cdot 15} \tag{A2.19}$$

$$|e_{\mathrm{tot}}| = \sqrt{|e|^2 + |e|^2 + 2 \cdot |e| \cdot |e|} = 2 \cdot e \tag{A2.20}$$

$$= \frac{2}{d} \sqrt{p_{\mathrm{tx}} \cdot g_{\mathrm{dip}} \cdot 15} \tag{A2.21}$$

$$= \frac{1}{d} \sqrt{p_{\mathrm{tx}} \cdot 90}. \tag{A2.22}$$

Appendix 3: Compensation for Measuring in the Near Field

Lorrain *et al.* [23], chapter 38, gives a good description of the near fields, electric and magnetic, of a small oscillating dipole. From there it is not difficult to derive equations that describe the distance function in the main radiation direction for the E- and H-field

$$|E| = \frac{[p]}{4\pi \in_0 \lambda\!\!\!^{-2} d} \sqrt{\left(\frac{\lambda\!\!\!^{-2}}{d^2} - 1\right)^2 + \left(\frac{\lambda\!\!\!^{-}}{d}\right)^2} \tag{A3.1}$$

$$= \frac{[p]}{4\pi \in_0 \lambda\!\!\!^{-2} d} \cdot k_E \tag{A3.2}$$

$$k_E = \sqrt{\left(\frac{\lambda\!\!\!^{-2}}{d^2} - 1\right)^2 + \left(\frac{\lambda\!\!\!^{-}}{d}\right)^2} \tag{A3.3}$$

$$|H| = \frac{c\,[p]}{4\pi \lambda\!\!\!^{-2}} \sqrt{(-1)^2 + \left(\frac{\lambda\!\!\!^{-}}{d}\right)^2} \tag{A3.4}$$

$$= \frac{c\,[p]}{4\pi \lambda\!\!\!^{-2}} \cdot k_H \tag{A3.5}$$

$$k_H = \sqrt{1 + \left(\frac{\lambda\!\!\!^{-}}{d}\right)^2} \tag{A3.6}$$

wherein k_E and k_E represents the correction factors in the near field for the electric, resp. the magnetic field component. In the far field with $d \gg \lambda$: $k_E = 1$ and $k_H = 1$. Herein the radian wavelength $\lambda\!\!\!^{-}$ is defined by

$$\lambda\!\!\!^{-} = \frac{\lambda}{2\pi}. \tag{A3.7}$$

REFERENCES

[1] T. W. H. Fockens, A. P. M. Zwamborn, and F. Leferink, "Measurements of the man-made noise floor on HF in the Netherlands," *IEEE Trans. Electromagn. Compat.*, vol. 61, no. 2, pp. 337–343, Apr. 2019, doi: 10.1109/TEMC.2018.2830512.

[2] T. W. H. Fockens and F. Leferink, "Correlation between measured man-made noise levels and the density of habitation," *IEEE Trans. Electromagn. Compat.*, vol. 62, no. 6, pp. 2696–2703, Dec. 2020, doi: 10.1109/TEMC.2020.3001979.

[3] J. Zenneck, "Propagation of plane EM waves along a plane conducting surface," *Ann. Phys. (Leipzig)*, vol. 28, pp. 846–866, 1907.

[4] A. N. Sommerfeld, "Propagation of waves in wireless telegraphy," *Ann. Phys. (Leipzig)*, vol. 28, pp. 665–737, 1909.

[5] K. A. Norton, "The propagation of radio waves over the surface of the earth and in the upper atmosphere, Part I," *Proc. IRE*, vol. 24, no. 10, pp. 1367–1387, Oct. 1936.

[6] K. A. Norton, "The propagation of radio waves over the surface of the earth and in the upper atmosphere, Part II," *Proc. IRE*, vol. 25, no. 9, pp. 1203–1236, Sep. 1937.

[7] K. A. Norton, "The physical reality of space and surface waves in the radiation field of radio antennas," *Proc. IRE*, vol. 25, no. 9, pp. 1192–1202, Sep. 1937.

[8] J. R. Wait, "The ancient and modern history of EM ground-wave propagation," *IEEE Antennas Propag. Mag.*, vol. 40, no. 5, pp. 7–24, Oct. 1998.

[9] R. E. Collin, "Hertzian dipole radiating over a lossy earth or sea: Some early and late 20th-century controversies," *IEEE Antennas Propag. Mag.*, vol. 46, no. 2, pp. 64–79, Apr. 2004.

[10] K. A. Norton, "The calculation of ground-wave field intensity over a finitely conducting spherical earth," *Proc. IRE*, vol. 29, no. 12, pp. 623–639, Dec. 1941.

[11] Ground-wave propagation curves for frequencies between 10 kHz and 30 MHz. Rec. ITU-R P.368-9, 2007. [Online]. Available: https://www.itu.int/rec/R-REC-P.368-9-200702-I/en

[12] Handbook on Ground Wave Propagation, ITU, 2014. [Online]. Available: https://www.itu.int/dms_pub/itu-r/opb/hdb/R-HDB-59-2014-PDF-E.pdf

[13] *GRWAVE*. Ground wave simulating tool from ITU-R. 2021. [Online]. Available: https://github.com/space-physics/grwave

[14] Y. Corre and Y. Lostanlen, "Three-dimensional urban EM wave propagation model for radio network planning and optimization over large areas," *IEEE Trans. Veh. Technol.*, vol. 58, no. 7, pp. 3112–3123, Sep. 2009, doi: 10.1109/TVT.2009.2016973.

[15] V. Degli-Esposti, "A diffuse scattering model for urban propagation prediction," *IEEE Trans. Antennas Propag.*, vol. 49, no. 7, pp. 111–1113, Jul. 2001.

[16] J. H. Causebrook, "Medium-wave propagation in built-up areas," *Proc. IEE*, vol. 125, no. 9, pp. 804–808, Sep. 1978.

[17] M. P. C. Almeida *et al.*, "Medium wave DRM field trials in Brazil - Some daytime and nighttime results in urban environment," *Measurement*, vol. 45, no. 9, pp. 2237–2245, 2012.

[18] M. J. Packer and R. I. Desourdis, "Rural and urban groundwave propagation in a desert environment," in *Proc. IEEE Mil. Commun. Conf.*, 1993, vol. 2, pp. 634–638.

[19] L. Lichun, "A new MF and HF ground-wave model for urban areas," *IEEE Antennas Propag. Mag.*, vol. 42, no. 1, pp. 21–33, Feb. 2000.

[20] The concept of transmission loss for radio links, Rec. ITU-R P.341-7, 2019. [Online]. Available: https://www.itu.int/rec/R-REC-P.341-7-201908-I/en

[21] F. J. Gravettes and L. B. Wallnau, *Statistics Behavioral Sci.*, 7th ed., Belmont, CA, USA: Thomson Wadsworth.

[22] *Antennas for all Applications*, 3rd ed. J. D. Kraus and R. J. Marhefka, Eds., New York, NY, USA: McGraw-Hill Higher Education, 2002.

[23] P. Lorrain, D. P. Corson, and F. Lorrain, *Electromagnetic Fields and Waves*, 3rd ed., New York, NY, USA: W. H. Freeman and Company, 1988.